An Improved Rotating Restart Method for a Sensorless Permanent-Magnet Synchronous Motor Drive System Using Repetitive Zero Voltage Vectors

Dong-Woo Seo, Yeongsu Bak, *Student Member, IEEE*,
and Kyo-Beum Lee, *Senior Member, IEEE*

***Abstract*—This paper presents an improved rotating restart method for a sensorless permanent-magnet synchronous motor (PMSM) drive system using repetitive zero voltage vectors. To restart the sensorless PMSM drive system, a method for estimating initial rotor position and speed is required due to the absence of sensors such as encoders and resolvers. The rotor position and speed can be estimated using the short-circuit current vectors generated by applying zero voltage vectors. However, the estimated rotor position and speed can be inaccurate. The inaccurate rotor position causes the current is distorted by the back electromotive force (EMF) of the PMSM and it is impossible to precisely control the system. Therefore, an improved rotating restart method for the sensorless PMSM drive system using repetitive zero voltage vectors is proposed. The effectiveness of the proposed method is verified through simulation and experimental results using a 5-kW PMSM drive system.**

***Index Terms*—Active neutral-point-clamped (ANPC) inverter, permanent-magnet synchronous motor (PMSM), repetitive zero voltage vectors, rotating restart method, sensorless control.**

I. Introduction

Recent development of an active neutral-point-clamped (ANPC) inverter has been undertaken in order to overcome the loss imbalance caused by the NPC inverter. It is used in various applications such as energy storage systems, adjustable-speed drives, and distributed generation [1]. In an adjustable-speed drives using the ANPC inverter, a permanent-magnet synchronous motor (PMSM) is often used due to its small size, low weight, high efficiency, and high power density. The PMSM drive system requires accurate measurement of rotor position and speed using various sensors such as encoders and resolvers. However, these sensors have the disadvantages of large system size, high cost, and low reliability due to disturbances. Recently, various sensorless control methods for the PMSM drive system are increasingly implemented in order to improve maintenance, convenience, and reliability [2]–[6].

There are two methods for sensorless PMSM drive system: one based on saliency and the other on electromotive force (EMF). The first sensorless control method based on the PMSM saliency uses high-frequency signal injection to estimate the rotor position. The high-frequency signal is injected into the rotating reference frame with a square waveform. It has advantages of highly reliable dynamic characteristics and system robustness, depending on the change of inductance. In addition, it exhibits good performance in the stationary or low-speed regime of the PMSM. However, the signal processing is complicated and the voltage margin of the inverter becomes insufficient when the PMSM speed increases [7]–[9]. The second sensorless control method estimates the rotor position and speed by modeling the PMSM through the extended EMF (EEMF). The sensorless PMSM drive system based on the EEMF estimates the rotor position through the error component, which is the difference between the estimated rotating reference frame and the real rotating reference frame with respect to the lowest-order observer. It has advantages of low computation requirement and simple control scheme structure [10]–[13].

In the PMSM drive systems, if the operation of the inverter is interrupted by an overload or abnormal system operation, the PMSM is controlled by the initial condition. If the PMSM drive systems operate with a sensor, it can restart without any additional control method because the rotor position and speed can be detected automatically by the sensor. However, the sensorless PMSM drive system cannot restart without information of the initial rotor position and speed of the PMSM. Therefore, an additional control method is required to estimate the initial PMSM rotor position and speed [14]–[16]. In general,

Manuscript received November 28, 2018; revised March 6, 2019; accepted April 3, 2019. This research was supported by a grant (No.20172020108970) from the Korea Institute of Energy Technology Evaluation and Planning (KETEP) that was funded by the Ministry of Trade, Industry and Energy (MOTIE) and the Korea Institute of Energy Technology Evaluation and Planning (KETEP) and the Ministry of Trade, Industry & Energy (MOTIE) of the Republic of Korea (No. 20171210201100). (*Corresponding author: Kyo-Beum Lee*)

D.-W. Seo is with the Power Grid Solution Division Power & Industrial System R&D Center, Hyosung, Seoul, 08592 South Korea (e-mail: sdw6737@hysung.com)

Y. Bak and K.-B. Lee are with the Department of Electrical and Computer Engineering, Ajou University, Suwon, 16499 South Korea (e-mail: wov2@ajou.ac.kr; kyl@ajou.ac.kr).

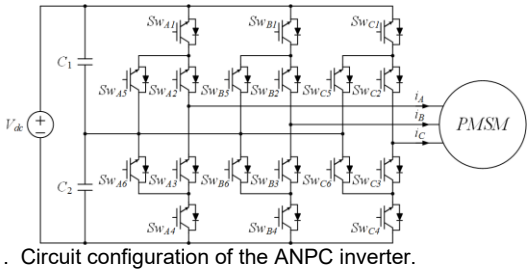

Fig. 1. Circuit configuration of the ANPC inverter.

TABLE I
ANPC SWITCHING STATES

Switching State	Sw_1	Sw_2	Sw_3	Sw_4	Sw_5	Sw_6	Voltage
P	1	1	0	0	0	1	$V_{dc}/2$
0U2	0	1	0	0	1	0	0
0U1	0	1	0	1	1	0	0
0L2	0	0	1	0	0	1	0
0L1	1	0	1	0	0	1	0
N	0	0	1	1	1	0	$-V_{dc}/2$

these are estimated by the conventional restart method that uses the short-circuit current vectors generated by one or two applied zero voltage vectors [17]−[20]. However, the estimated initial rotor position and speed of the PMSM can be inaccurate due to the problems such as error of measured short-circuit currents. It causes that the dynamic response and performance of the sensorless PMSM drive system can deteriorate [21]–[23].

In this paper, an improved rotating restart method for the sensorless PMSM drive system based on the EEMF using an ANPC inverter is proposed. In order to estimate accurate initial rotor position and speed during the restart operation, repetitive zero voltage vectors are used and the number of repetitions is selected through the average value and differences of the speed estimated by the repetitive zero voltage vectors. In addition, the proposed method using the repetitive zero voltage vectors for improved rotating restart method is valid for sensorless PMSM drive systems using various topologies as well as ANPC inverter. The effectiveness of the proposed rotating restart method is verified by the simulation and experimental results.

II. SENSORLESS PMSM DRIVE SYSTEM

A. Circuit Configuration

Fig. 1 shows the circuit configuration of the ANPC inverter, composed of six switches on a leg. The switching states are presented in Table I. The ANPC inverter has balanced switching losses because the zero switching states (0U2, 0U1, 0L2, 0L1) use the two clamped switches (Sw_5, Sw_6), thereby increasing the efficiency of the system using the ANPC inverter. Additionally, the filter size and the current harmonic components can be decreased in this configuration.

B. PMSM Modeling

Fig. 2 shows the vector diagram of the PMSM and different coordinate axes. In Fig. 2, the α^s–β^s axis is the stationary reference frame, the d^r–q^r axis is the rotating reference frame, the γ–δ axis is the estimated rotating reference frame, and $\hat{\theta}_{err}$ is the phase angle between the d^r–q^r axis and γ–δ axis. The voltage equations of the PMSM in the α^s–β^s axis and the d^r–q^r axis are expressed as in (1) and (2), respectively.

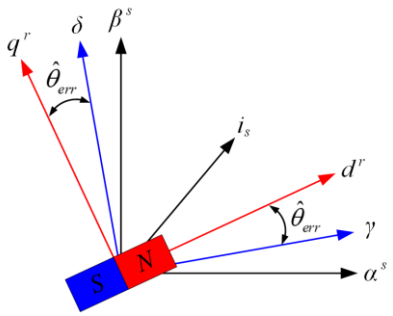

Fig. 2. Vector diagram of PMSM and different coordinate axes.

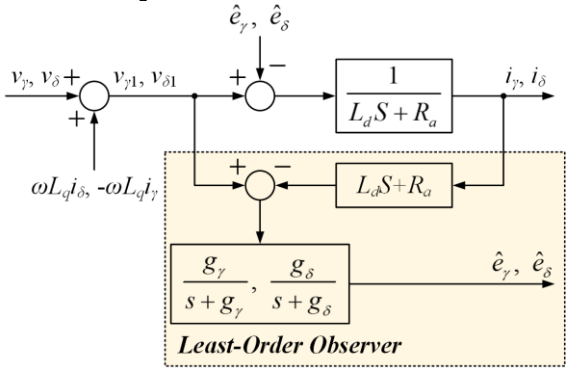

Fig. 3. EEMF estimation block diagram using the least-order observer.

$$\begin{bmatrix} v_\alpha^s \\ v_\beta^s \end{bmatrix} = \begin{bmatrix} R_a + p\left(L_0 + L_1\cos 2\theta_e\right) & pL_1 \sin 2\theta_e \\ pL_1 \sin 2\theta_e & R_a + p\left(L_0 - L_1\cos 2\theta_e\right) \end{bmatrix} \begin{bmatrix} i_\alpha^s \\ i_\beta^s \end{bmatrix} + \omega_e \phi_a \begin{bmatrix} -\sin\theta_e \\ \cos\theta_e \end{bmatrix}, \quad L_0 = \frac{(L_d + L_q)}{2}, \quad L_1 = \frac{(L_d - L_q)}{2}, \tag{1}$$

$$\begin{bmatrix} v_d^r \\ v_q^r \end{bmatrix} = \begin{bmatrix} R_a + pL_d & -\omega_e L_q \\ \omega_e L_d & R_a + pL_q \end{bmatrix} \begin{bmatrix} i_d^r \\ i_q^r \end{bmatrix} + \begin{bmatrix} 0 \\ \omega_e \phi_a \end{bmatrix}, \tag{2}$$

where v^s_α and v^s_β are α^s–β^s axis stator voltages, i^s_α and i^s_β are α^s–β^s axis armature currents, R_a is armature resistance, L_d and L_q are d–q axis inductance values, p is a differential operator, ω_e is rotor angular frequency, ϕ_a is magnet flux linkage, and θ_e is rotor position. v^r_d and v^r_q are d^r–q^r axis stator voltages and i^r_d and i^r_q are d^r–q^r axis armature currents. In (1) and (2), a linear PMSM is only considered for modeling rather than a real PMSM. Additionally, an iron saturation of the PMSM is neglected.

C. EEMF Voltage Modeling

The voltage equations of the PMSM using the EMF of the PMSM (E_{emf}), which is defined according to (4), in the α^s–β^s axis and the d^r–q^r axis are expressed as in (3) [10].

$$\begin{bmatrix} v_\alpha^s \\ v_\beta^s \end{bmatrix} = \begin{bmatrix} R_a + pL_d & \omega_e(L_d - L_q) \\ -\omega_e(L_d - L_q) & R_a + pL_d \end{bmatrix} \begin{bmatrix} i_\alpha^s \\ i_\beta^s \end{bmatrix} + E_{emf} \begin{bmatrix} -\sin\theta_e \\ \cos\theta_e \end{bmatrix},$$
$$\begin{bmatrix} v_d^r \\ v_q^r \end{bmatrix} = \begin{bmatrix} R_a + pL_d & -\omega_e L_q \\ \omega_e L_q & R_a + pL_d \end{bmatrix} \begin{bmatrix} i_d^r \\ i_q^r \end{bmatrix} + \begin{bmatrix} 0 \\ E_{emf} \end{bmatrix}. \tag{3}$$

$$E_{emf} = \omega_e\left[(L_d - L_q) i_d^r + \phi_a\right] - (L_d - L_q) p i_q^r. \tag{4}$$

This article has been accepted for publication in a future issue of this journal, but has not been fully edited. Content may change prior to final publication. Citation information: DOI 10.1109/TIE.2019.2914647, IEEE Transactions on Industrial Electronics

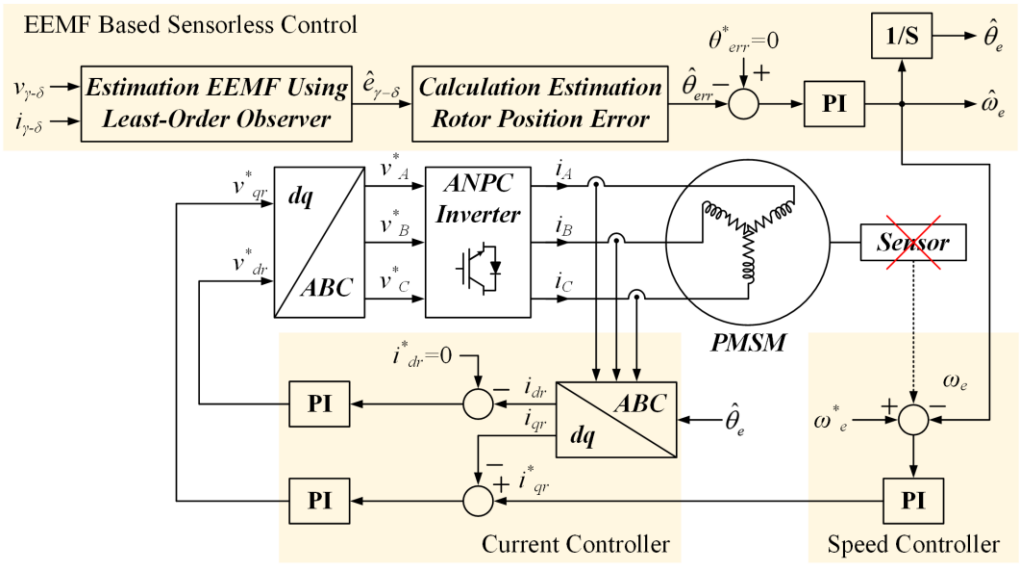

Fig. 4. Control block diagram of sensorless PMSM drive system based on the EEMF using the ANPC inverter.

If the phase angle between the d^r–q^r axis and γ–δ axis is negligibly small, the rotor position and speed of the PMSM can be estimated. From (3), the voltage equation of the PMSM in the γ–δ axis can then be expressed as in (5).

$$\begin{bmatrix} v_\gamma \\ v_\delta \end{bmatrix} = \begin{bmatrix} R_a + pL_d & -\omega_e L_q \\ \omega_e L_q & R_a + pL_d \end{bmatrix} \begin{bmatrix} i_\gamma \\ i_\delta \end{bmatrix} + \begin{bmatrix} e_\gamma \\ e_\delta \end{bmatrix}, \tag{5}$$

where e_γ and e_δ are the EEMF values in the γ–δ axis, which are expressed as in (6).

$$\begin{bmatrix} e_\gamma \\ e_\delta \end{bmatrix} = E_{emf} \begin{bmatrix} -\sin\hat{\theta}_{err} \\ \cos\hat{\theta}_{err} \end{bmatrix} + \left(\hat{\omega}_e - \omega_e\right) L_d \begin{bmatrix} -i_\gamma \\ i_\delta \end{bmatrix}. \tag{6}$$

Fig. 3 shows the EEMF estimation block diagram where $g_{\gamma\text{–}\delta}$ is the gain of the least-order observer, which is used to obtain the estimated e_γ and e_δ values ($\hat{e}_\gamma$ and $\hat{e}_\delta$). If the error between the estimated and real rotor speed ($\hat{\omega}_e$ and ω_e) is negligibly small, $\hat{\theta}_{err}$, the phase angle between the d^r–q^r axis and γ–δ axis, can be expressed as in (7).

$$\hat{\theta}_{err} = \tan^{-1}\left(\frac{-\hat{e}_\gamma}{\hat{e}_\delta}\right). \tag{7}$$

Fig. 4 shows the control block diagram of the sensorless PMSM drive system based on the EEMF using the ANPC inverter. First, the phase angle $\hat{\theta}_{err}$ expressed as in (7) is set to zero using the proportional-integral (PI) controller and $\hat{\omega}_e$ and $\hat{\theta}_e$, the estimated rotor position and speed are obtained. The $\hat{\omega}_e$ and $\hat{\theta}_e$ are used for the speed control and coordinate transformation of the three-phase currents (i_A, i_B, and i_C), respectively. The PMSM rotor speed is controlled using the reference rotor speed (ω^*_e) and $\hat{\omega}_e$, and the output value of the speed controller is the q^r–axis reference current (i^*_{qr}). The d^r–axis reference current (i^*_{dr}) is set to zero and the d^r–q^r axis output currents of the PMSM (i_{dr} and i_{qr}) are controlled by the i^*_{dr} and i^*_{qr}, respectively. Finally, the ANPC inverter operates according to the reference voltages (v^*_{dr} and v^*_{qr}), which are the output values of the current controller.

III. Improved Rotating Restart Method for the Sensorless PMSM Drive System

When the operation of the inverter in the sensorless PMSM drive system is interrupted, it cannot restart without information of the PMSM rotor position and speed. Various studies of the rotating restart method have investigated as a result.

A. Conventional Method using Two Zero Voltage Vectors

In the conventional rotating restart method, the zero voltage vectors are applied by the inverter during sampling time T to estimate the initial PMSM rotor position and speed [15]. Depending on these zero voltage vectors, short-circuit currents are generated by the back-EMF of the PMSM that are then used to estimate the initial rotor position and speed of the PMSM.

If the T is sufficiently small compared to the q^r–axis time constant, R_a in the voltage equation of the PMSM as described by (2) can be considered zero. The voltage equation with zero voltage vectors can therefore be expressed as in (8).

$$\begin{bmatrix} 0 \\ 0 \end{bmatrix} = \begin{bmatrix} pL_d & -\omega_e L_q \\ \omega_e L_d & pL_q \end{bmatrix} \begin{bmatrix} i^r_d \\ i^r_q \end{bmatrix} + \begin{bmatrix} 0 \\ \omega_e \phi_a \end{bmatrix}. \tag{8}$$

From (8), if the ω_e is constant and the initial current is zero, the i^r_d and i^r_q can be converted to $i_{SC}(T)$, the short-circuit current vector, as expressed as in (9) using the Laplace transform.

$$i_{SC}(T) = \begin{bmatrix} i^r_d(T) \\ i^r_q(T) \end{bmatrix} = \begin{bmatrix} -\dfrac{\phi_a}{L_d}(1-\cos\omega_e T) \\ -\dfrac{\phi_a}{L_q}\sin\omega_e T \end{bmatrix}. \tag{9}$$

Fig. 5 shows the short-circuit current vectors generated by first and second zero voltage vectors. When the first zero voltage vector is applied by the inverter, the short-circuit current vector $i_{SC1}(T)$ is generated. In the variable $i_{SC1}(T)$, the subscript number means the number of zero voltage vector and

This article has been accepted for publication in a future issue of this journal, but has not been fully edited. Content may change prior to final publication. Citation information: DOI 10.1109/TIE.2019.2914647, IEEE Transactions on Industrial Electronics

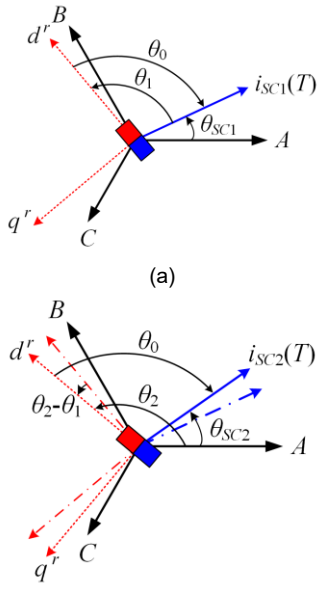

Fig. 5. Short-circuit current vectors generated by (a) first and (b) second zero voltage vectors.

the T in the bracket means the applying time of the zero voltage vector. Therefore, the $i_{SCn}(T)$ means the short-circuit current vector generated by the applied n-th zero voltage vector during sampling time T. The θ_0 is phase angle between the initial rotor position d^r–axis and the $i_{SC1}(T)$, and the θ_1 is phase angle between the A–axis and the d^r–axis. In addition, θ_{SC1} is angular difference between the A–axis and the $i_{SC1}(T)$. The value of θ_0 is given by (10).

$$\theta_0 \cong \tan^{-1}\left(\frac{i_q^r}{i_d^r}\right) = \tan^{-1}\left(\frac{-\frac{\phi_a}{L_q}\sin\omega_e T}{-\frac{\phi_a}{L_d}\left(1-\cos\omega_e T\right)}\right) = \tan^{-1}\left(\frac{L_d \sin\omega_e T}{L_q\left(1-\cos\omega_e T\right)}\right). \quad (10)$$

The θ_{SC1} is obtained by converting the three-phase currents into the α^s–β^s axis components and it is expressed as in (11).

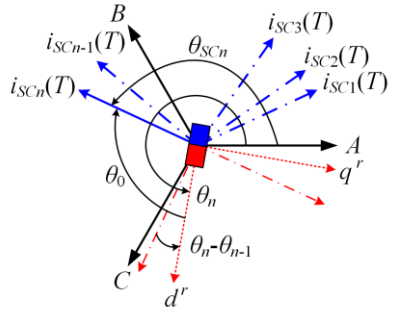

Fig. 6. Short-circuit current vectors generated by repetitive zero voltage vectors.

$$\theta_{SC1} \approx \tan^{-1}\left(\frac{i_\beta^s}{i_\alpha^s}\right). \quad (11)$$

Therefore, θ_1, the initial rotor position of the PMSM, is calculated as θ_{SC1}-θ_0. However, the θ_1 estimated by the first zero voltage vector includes an error component in the initial rotor position of the PMSM. The second zero voltage vector is therefore applied by the inverter and the second short-circuit current vector $i_{SC2}(T)$ is generated as shown in Fig. 5(b). Finally, the estimated initial rotor speed (ω_{est}) of the PMSM is calculated according to (12) by using the θ_{SC1} and θ_{SC2}, which are obtained through $i_{SC1}(T)$ and $i_{SC2}(T)$.

$$\omega_{est} = \frac{\theta_{SC2} - \theta_{SC1}}{T + \tau}, \quad (12)$$

where τ is time interval between the first and second zero voltage vector. It is required to ensure that the next zero voltage vector is applied after the short-circuit current vector goes to zero. The maximum value of the τ depends on the short-circuit duration, amplitude of back-EMF, and the stator winding time constants [15].

When the conventional rotating restart method is used, the estimated rotor position and speed of the PMSM can be inaccurate due to the problems such as error of measured short-circuit currents. The inaccurate rotor position causes the current is distorted by the back-EMF of the PMSM and it is impossible to precisely control the system. Therefore, in this paper, an improved method using repetitive zero voltage vectors for accurate estimation of the initial rotor position and speed is proposed.

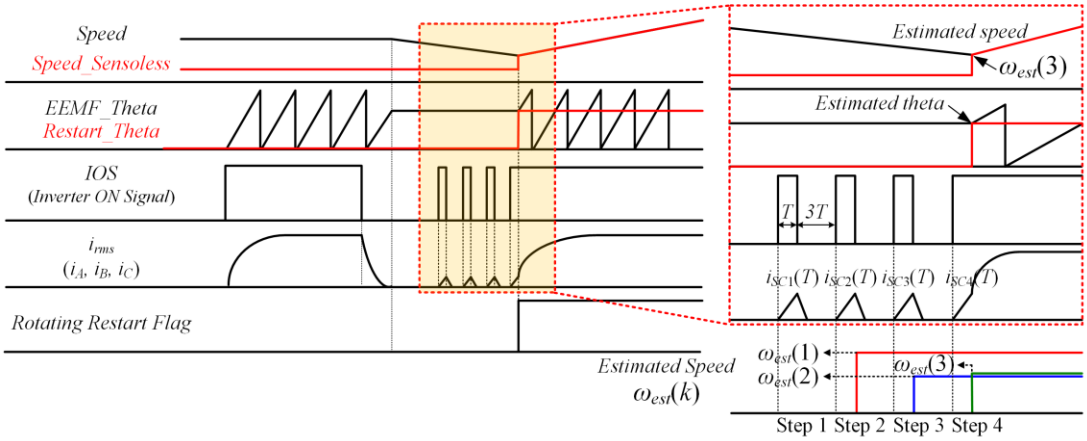

Fig. 7. Conceptual diagram of the improved rotating restart method using repetitive zero voltage vectors.

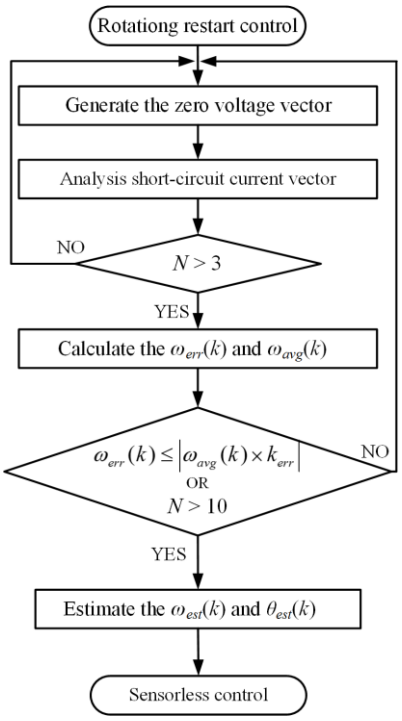

Fig. 8. Flowchart of improved rotating restart method using repetitive zero voltage vectors.

B. Improved Method using Repetitive Zero Voltage Vectors

In the improved rotating restart method, the repetitive zero voltage vectors are applied by the inverter for more accurate estimation of the rotor position and speed of the PMSM. As in the conventional rotating restarting method, the short-circuit currents of the PMSM are detected by the current sensors and are used to estimate the initial rotor position and speed of the PMSM. The first zero voltage vector is applied by the inverter during sampling time T, and the second zero voltage vector is applied after a time interval of $3T$. This process is repeated multiple times.

Fig. 6 shows the short-circuit current vectors generated by the repetitive zero voltage vectors. In Fig. 6, the $i_{SCn}(T)$ is the short-circuit current vector where subscript n is the number of repetitive zero voltage vectors. When the n-th zero voltage vector is applied, the θ_{SCn} is phase angle of the short-circuit current vector and the θ_0 is the phase angle between the initial rotor position d^r–axis and the $i_{SCn}(T)$. Additionally, the θ_n is the phase angle between the A–axis and the d^r–axis and the estimated rotor position $\theta_{est}(k)$ of the PMSM is calculated as θ_{SCn}-θ_0 using (10) and (11). Finally, the initial rotor position and speed of the PMSM can be accurately obtained by using the error in ω and the average value of ω_{est}.

The detailed conceptual diagram of the improved rotating restart method is shown in Fig. 7. When the operation of the inverter in the sensorless PMSM drive system is interrupted, the *Inverter ON Signal* (*IOS*) is set to zero. In Fig. 7, the rotor speed of the PMSM and the three-phase currents (i_A, i_B, and i_C) expressed as in i_{rms} decrease and the rotor position (*EEMF_Theta*) cannot be obtained by the sensorless control method based on the EEMF. In order to restart the sensorless PMSM drive system with the improved rotating restart method,

TABLE II
PARAMETERS OF PMSM

Parameter	Value
Rated power	5 kW
Rated current	19.09 A
Rated speed	1750 rpm
Rated torque	27.3 Nm
Number of poles	4
Stator resistance	0.158 Ω
d-axis inductance	0.00729 H
q-axis inductance	0.00725 H
Permanent magnet flux	0.26401 Wb
Moment of inertia	0.006 kgm^2

the zero voltage vectors are applied by the inverter with the high value of the *IOS* as shown in Fig. 7. The short-circuit currents are generated by the zero voltage vectors and the initial rotor position and speed are estimated by the improved rotating restart method, which is explained with reference to Fig. 7 as follows:

Step 1: the first zero voltage vector is applied by the inverter for time T. The inverter is turned off for a period of $3T$ until the short-circuit current goes to zero. At this time, $\theta_{est}(1)$, the rotor position of the PMSM, is estimated using the short-circuit current vector $i_{SC1}(T)$.

Step 2: the second zero voltage vector is applied by the inverter for time T in order to obtain the $\theta_{est}(2)$ using the $i_{SC2}(T)$. In addition, $\omega_{est}(1)$, the rotor speed of the PMSM, is estimated using the phase angle between $\theta_{est}(1)$ and $\theta_{est}(2)$. If the estimated rotor position and speed of the PMSM are inaccurate due to the problems such as error of measured short-circuit currents, it causes problems for successfully restarting the sensorless PMSM drive system.

Step 3: as in the above steps, the values of $\theta_{est}(3)$ and $\omega_{est}(2)$ are estimated using the $i_{SC3}(T)$. Additionally, $\omega_{avg}(1)$, the average value of $\omega_{est}(1)$ and $\omega_{est}(2)$, is defined and calculated by the speed ($\omega_{est}(k\text{-}1)$ and $\omega_{est}(k)$) estimated at the present and previous step, respectively, according to (13).

$$\omega_{avg}(k) = \frac{\omega_{est}(k-1) + \omega_{est}(k)}{2}. \tag{13}$$

Step 4: the $\theta_{est}(4)$ and $\omega_{est}(3)$ are estimated using the $i_{SC4}(T)$ and the $\omega_{avg}(2)$ is calculated with the $\omega_{est}(2)$ and $\omega_{est}(3)$. Finally, the rotor position and speed can be accurately obtained using the evaluation criteria of the estimated speed, which are expressed in (14).

$$\begin{aligned} &\omega_{err}(k) = \left|\omega_{avg}(k) - \omega_{est}(k)\right|, \\ &\omega_{err}(k) \le \left|\omega_{avg}(k) \times k_{err}\right|, \end{aligned} \tag{14}$$

where $\omega_{err}(k)$ is the estimated speed error, which is the difference between $\omega_{avg}(k)$ and $\omega_{est}(k)$, and k_{err} is the speed evaluation error constant, which is set to 3–5%. It is determined depending on the requirements of the system users. In this paper, if $\omega_{err}(k)$ is less than 5% of $\omega_{avg}(k)$, it is assumed that the PMSM rotor speed is sufficiently accurately estimated. Finally, the $\omega_{est}(k)$ is used in the feed-forward components of the sensorless PMSM drive system. However, if the estimated rotor position and speed are inaccurate, this process is repeated from Step 3 to Step 4 in order to estimate the optimum rotor position and speed.

This article has been accepted for publication in a future issue of this journal, but has not been fully edited. Content may change prior to final publication. Citation information: DOI 10.1109/TIE.2019.2914647, IEEE Transactions on Industrial Electronics

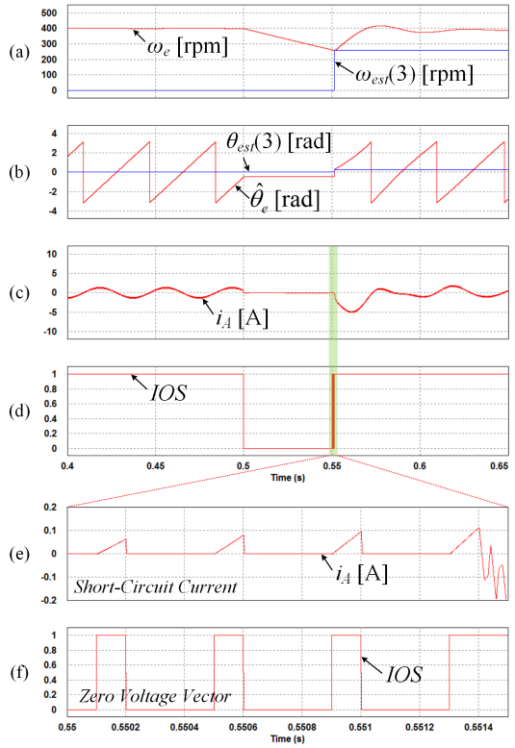

Fig. 9. Simulation results of the improved rotating restart method applying four zero voltage vectors where the PMSM is rotated at 400 rpm. (a) rotor speed and estimated initial rotor speed. (b) rotor position and estimated initial rotor position. (c) *A*-phase current. (d) IOS of the ANPC inverter. (e) magnified i_A. (f) IOS waveform.

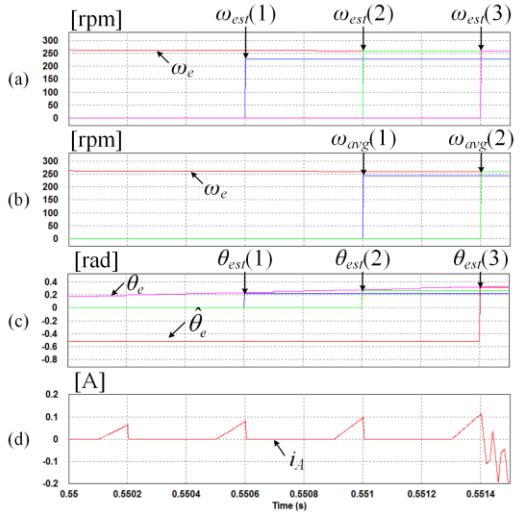

Fig. 10. Simulation results of the estimated initial rotor position and speed where the PMSM is rotated at 400 rpm. (a) estimated initial rotor speed. (b) average value of estimated initial rotor speed. (c) estimated initial rotor position. (d) *A*-phase current.

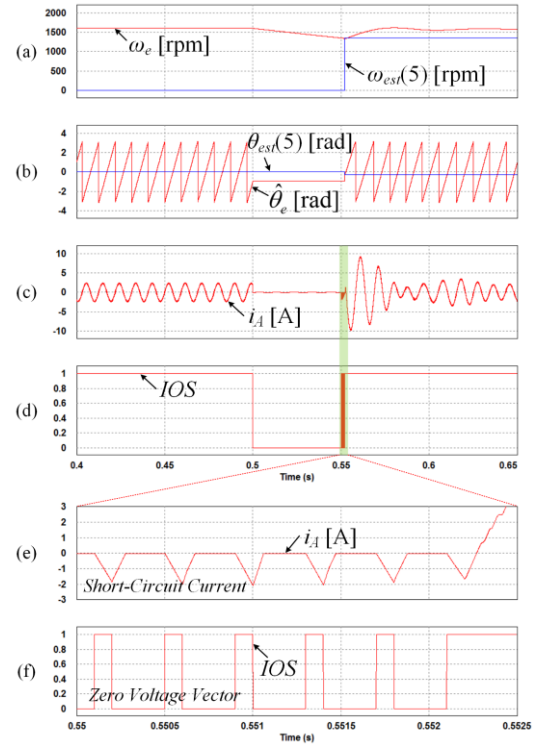

Fig. 11. Simulation results of the improved rotating restart method applying six zero voltage vectors where the PMSM is rotated at 1600 rpm. (a) rotor speed and estimated initial rotor speed. (b) rotor position and estimated initial rotor position. (c) *A*-phase current. (d) IOS of the ANPC inverter. (e) magnified i_A. (f) IOS waveform.

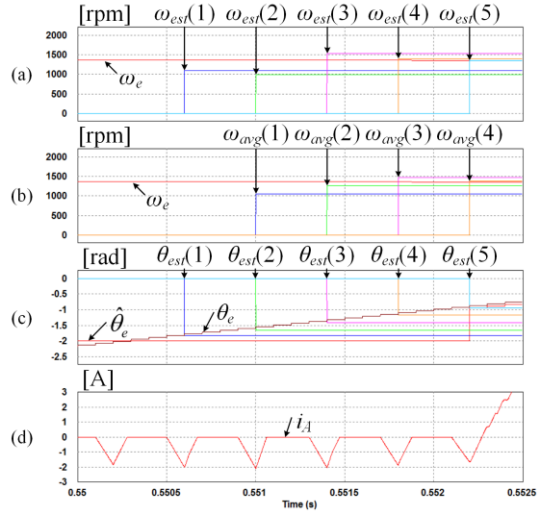

Fig. 12. Simulation results of the estimated initial rotor position and speed where the PMSM is rotated at 1600 rpm. (a) estimated initial rotor speed. (b) average value of estimated initial rotor speed. (c) estimated initial rotor position. (d) *A*-phase current.

Fig. 8 shows the flowchart of the improved rotating restart method using the repetitive zero voltage vectors, where N is the number of times that the zero voltage vector is applied.

IV. Simulation Results

The effectiveness of the improved rotating restart method of the sensorless PMSM drive system using the repetitive zero voltage vectors is verified by the PSIM simulation results. The proposed method is valid for sensorless PMSM drive systems using various topologies. However, in this paper, the ANPC inverter as shown in Fig. 1 is used for the PMSM drive system as the power conversion device. The parameters of the PMSM used in the simulation are presented in Table II.

Fig. 9 shows the simulation results of the improved rotating restart method applying four zero voltage vectors where the PMSM is rotated at 400 rpm. Fig. 9(a) shows the rotor speed (ω_e) obtained from the encoder, and $\omega_{est}(3)$, the initial rotor speed estimated using the improved rotating restart method. Fig.

This article has been accepted for publication in a future issue of this journal, but has not been fully edited. Content may change prior to final publication. Citation information: DOI 10.1109/TIE.2019.2914647, IEEE Transactions on Industrial Electronics

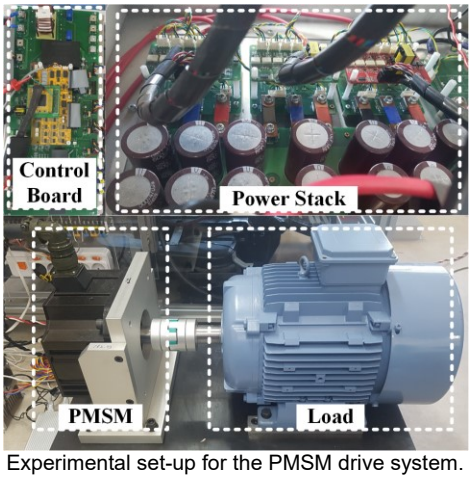

Fig. 13. Experimental set-up for the PMSM drive system.

9(b) shows $\hat{\theta}_e$, the rotor position found using the sensorless control method based on the EEMF, and $\theta_{est}(3)$, the initial rotor position estimated using the improved rotating restart method. Fig. 9(c) shows the A-phase current (i_A) of the PMSM and Fig. 9(d) shows the operating state (IOS) of the ANPC inverter. Figs. 9(e) and (f) show the magnified i_A and IOS waveforms, which represent the short-circuit current and the zero voltage vector, respectively. As shown in Fig. 9, the operation of the ANPC inverter stops at 0.5 s and the improved rotating restart method is applied at 0.55 s. The zero voltage vectors are applied by the ANPC inverter four times, each for duration T, to generate the short-circuit currents. The initial rotor position ($\theta_{est}(3)$) and speed ($\omega_{est}(3)$) of the PMSM are estimated as shown in Figs. 9(a) and (b).

Fig. 10 shows the simulation results of the estimated initial rotor position and speed where the PMSM is rotated at 400 rpm. Fig. 10(a) shows the $\omega_{est}(k)$ estimated by each short-circuit current vector. Fig. 10(b) shows the $\omega_{avg}(k)$ calculated from $\omega_{est}(k)$ and $\omega_{est}(k\text{-}1)$. Fig. 10(c) and (d) show the $\theta_{est}(k)$ with θ_e as the real rotor position and the i_A, respectively. In Fig. 10(c), the $\theta_{est}(k)$ is the phase angle of the d^r–axis when the n-th zero voltage vector is applied. The $\omega_{est}(1)$ estimated by using the the first and second short-circuit current is inaccurate compared to the ω_e. Therefore, the repetitive zero voltage vectors are applied for the improved rotating restart method. Since the $\omega_{err}(k)$ should be satisfied as in (14), the short-circuit current is applied up to four times. Finally, the $\omega_{est}(3)$ and $\theta_{est}(3)$ are estimated by using the repetitive zero voltage vectors, which are applied to the feed-forward components of the sensorless control method.

Fig. 11 shows the simulation results of the improved rotating restart method applying six zero voltage vectors where the PMSM is rotated at 1600 rpm, displaying the same scenario as that of Fig. 9. In this case the short-circuit currents are generated by the six zero voltage vectors. The $\theta_{est}(5)$ and $\omega_{est}(5)$ are accurately estimated.

Fig. 12 shows the simulation results of the estimated initial rotor position and speed where the PMSM is rotated at 1600 rpm, featuring the same scenario as that of Fig. 10. In Fig. 12, the estimated rotor speeds are inaccurate while the five zero voltage vectors are applied, until the $\omega_{err}(k)$ satisfies as in (14). Finally, the $\omega_{est}(5)$ and $\theta_{est}(5)$ are estimated by using the repetitive zero voltage vectors, which are applied to the feed-forward components of the sensorless control method.

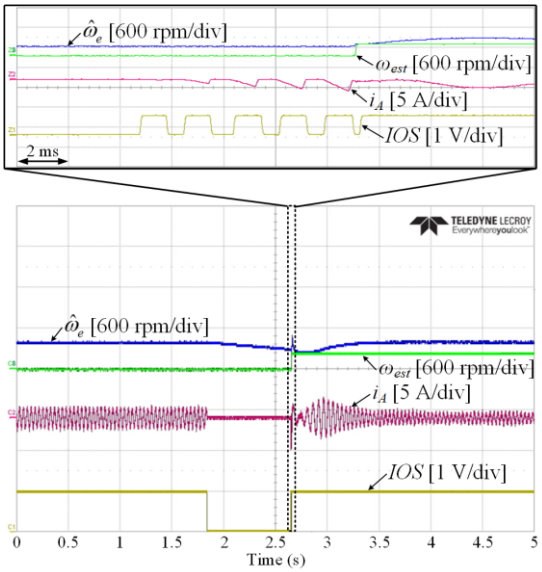

Fig. 14. Experimental results of the improved rotating restart method applying six zero voltage vectors where the PMSM is rotated at 400 rpm.

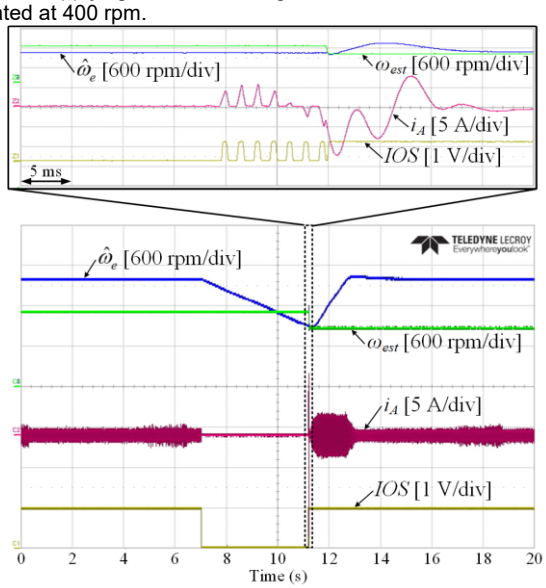

Fig. 15. Experimental results of the improved rotating restart method applying eight zero voltage vectors where the PMSM is rotated at 1600 rpm.

V. Experimental Results

Experiments were conducted to verify the effectiveness of the improved rotating restart method of the sensorless PMSM drive system using the ANPC inverter. Fig. 13 shows the experimental set-up for the PMSM drive system, consisting of the control board, ANPC power stack, PMSM, and the load. The control board is comprised of a digital signal processor (DSP) using a TMS320F28377 and the control algorithms for the improved rotating restart method is programmed into the DSP. The sampling time T in the experimental set-up is 100 μs and the interval time τ is set to $3T$. The ANPC inverter is comprised of insulated-gate bipolar transistors (IGBTs), gate drivers, and DC-link capacitors. The parameters of the PMSM are identical to those listed in Table II.

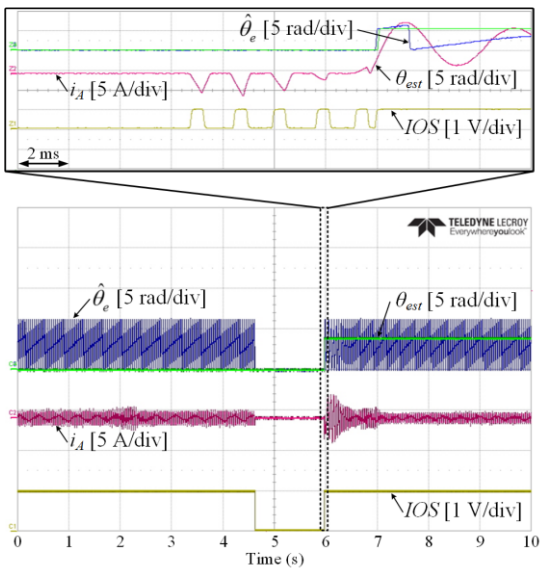

Fig. 16. Experimental results of estimated initial rotor position where the PMSM is rotated at 1600 rpm.

Fig. 14 shows the experimental results of the improved rotating restart method applying six zero voltage vectors where the PMSM is rotated at 400 rpm. The ANPC inverter stops operating at 1.8 s and the improved rotating restart method is applied at 2.7 s. The six zero voltage vectors are applied by the ANPC inverter each for time T to generate the short-circuit currents. As a result, the $\omega_{est}(5)$ is accurately estimated using the short-circuit currents and it is applied to the feed-forward component of the sensorless control method so that the sensorless PMSM drive system can be restarted.

Fig. 15 shows the experimental results of the improved rotating restart method applying eight zero voltage vectors where the PMSM is rotated at 1600 rpm, showing the same scenario as that of Fig. 14. In this case the eight zero voltage vectors are applied by the ANPC inverter. Since the estimated rotor speed of the PMSM are inaccurate until $\omega_{err}(k)$ satisfies as in (14), the zero voltage vectors are repeatedly applied by the ANPC inverter in order to generate the short-circuit currents. As a result, the $\omega_{est}(8)$ is accurately estimated and it is applied to the feed-forward component of the sensorless control method so that the sensorless PMSM drive system can be restarted.

Fig. 16 shows the experimental results of the estimated initial rotor position where the PMSM is rotated at 1600 rpm. The θ_{est} is estimated using the sixth short-circuit current vector and it is applied to the feed-forward component of the sensorless control method.

VI. Conclusion

This paper proposes an improved rotating restart method for the sensorless PMSM drive system using repetitive zero voltage vectors. In order to restart the sensorless PMSM drive system, the initial rotor position and speed of the PMSM are required. These can be estimated using the short-circuit current vectors generated by the zero voltage vectors. However, due to the problems such as error of measured short-circuit currents, the estimated rotor position and speed can be inaccurate. The inaccurate rotor position causes the current is distorted by the back electromotive force (EMF) of the PMSM and it is impossible to precisely control the system. Therefore, in order to estimate the accurate initial rotor position and speed of the PMSM, the improved rotating restart method using the repetitive zero voltage vectors is proposed in this paper. The proposed scheme using the repetitive zero voltage vectors for improved rotating restart method is valid for sensorless PMSM drive systems using various topologies as well as ANPC inverter. The effectiveness of the proposed method was successfully verified by the simulation and experimental results.

References

[1] T. Bruckner, S. Bernet, and H. Guldner, "The active NPC converter and its loss-balancing control," *IEEE Trans. Ind. Electron.*, vol. 52, no. 3, pp. 855–868, Jun. 2005.

[2] Y. Bak and K.-B. Lee, "Reverse matrix converter control method for PMSM drives using DPC," *International Journal of Electronics*, vol. 105, no. 5, pp. 725–740, May 2018.

[3] H. Kim, J. Son, and J. Lee "A high-speed sliding-mode observer for the sensorless speed control of a PMSM," *IEEE Trans. Ind. Electron.*, vol. 58, no. 9, pp. 4069–4077, Sep. 2011.

[4] S.-K. Kim, J.-S. Lee, and K.-B. Lee, "Robust speed control algorithm with disturbance observer for uncertain PMSM," *International Journal of Electronics*, vol. 105, no. 8, pp. 1300–1318, Aug. 2018.

[5] S. Bolognani, R. Oboe, and M. Zigliotto, "Sensorless full-digital PMSM drive with EKF estimation of speed and rotor position," *IEEE Trans. Ind. Electron.*, vol. 46, no. 1, pp. 184–191, Feb. 1999.

[6] Y. Bak, E. Lee, and K.-B. Lee, "Indirect matrix converter for hybrid electric vehicle application with three-phase and single-phase outputs," *Energies*, vol. 8, no. 5, pp. 3849–3866, Apr. 2015.

[7] Y.-D. Yoon, S.-K. Sul, S. Morimoto, and K. Ide, "High-bandwidth sensorless algorithm for AC machines based on square-wave-type voltage injection," *IEEE Trans. Ind. Appl.*, vol. 47, no. 3, pp. 1361–1370, May/Jun. 2011.

[8] X. Luo, Q. Tang, A Shen, and Q. Zhang "PMSM sensorless control by injecting HF pulsating carrier signal into estimated fixed-frequency rotating reference frame," *IEEE Trans. Ind. Electron.*, vol. 63, no. 4, pp. 2294–2303, Apr. 2016.

[9] X. Zhang, H. Li, S. Yang, and M. Ma, "Improved initial rotor position estimation for PMSM drives based on HF pulsating voltage signal injection," *IEEE Trans. Ind. Electron.*, vol. 65, no. 6, pp. 4702–4713, Jun. 2018.

[10] S. Morimoto, K. Kawamoto, M. Sanada, and Y. Takeda, "Sensorless control strategy for salient-pole PMSM based on extended EMF in rotating reference frame," *IEEE Trans. Ind. Appl.*, vol. 38, no. 4, pp. 1054–1061, Jul./Aug. 2002.

[11] F. Genduso, R. Miceli, C. Rando, and G. R. Galluzzo, "Back EMF sensorless-control algorithm for high-dynamic performance PMSM," *IEEE Trans. Ind. Electron.*, vol. 57, no. 6, pp. 2092–2100, Jun. 2010.

[12] K. Wang, B. Chen, G. Shen, W. Yao, K. Lee, and Z. Lu, "Online updating of rotor time constant based on combined voltage and current mode flux observer for speed-sensorless AC drives," *IEEE Trans. Ind. Electron.*, vol. 61, no. 9, pp. 4583–4593, Sep. 2014.

[13] K. Ide, J.-I. Ha, and M. Sawamura, "A hybrid speed estimator of flux observer for induction motor drives," *IEEE Trans. Ind. Electron.*, vol. 53, no. 1, pp. 130–137, Feb. 2006.

[14] J.-I. Ha, K. Ide, T. Sawa, and S.-K. Sul, "Sensorless rotor position estimation of an interior permanent-magnet motor from initial states," *IEEE Trans. Ind. Appl.*, vol. 39, no. 3, pp. 761–767, May/Jun. 2003.

[15] S. Taniguchi, S. Mochiduki, T. Yamakawa, S. Wakao, K. Kondo, and T. Yoneyama, "Starting procedure of rotational sensorless PMSM in the rotating condition," *IEEE Trans. Ind. Appl.*, vol. 45, no. 1, pp. 194–202, Jan./Feb. 2009.

[16] T. Aihara, A. Toba, T. Yanase, A. Mashimo, and K. Endo, "Sensorless torque control of salient-pole synchronous motor at zero-speed operation," *IEEE Trans. Power Electron.*, vol. 14, no. 1, pp. 202–208, Jan. 1999.
[17] R. Raute, C. Caruana, J. Cilia, C. S. Staines, M. Sumner, "A zero speed operation sensorless PMSM drive without additional test signal injection," *in Proc. EPE Conf.*, pp. 1–10, 2007.
[18] K. Lee, S. Ahmed, and S. M. Lukic, "Universal restart strategy for high-inertia scalar-controlled PMSM drives," *IEEE Trans. Ind. Appl.*, vol. 52, no. 5, pp. 4001–4009, Sep./Oct. 2016.
[19] H. Yang, Y. Zhang, P. D. Walker, N. Zhang, and B. Xia "A method to start rotating induction motor based on speed sensorless model-predictive control," *IEEE Trans. Energy Convers.*, vol. 32, no. 1, pp. 359–368, Mar. 2017.
[20] T. Horie and K. Kondo, "Experimental study on a restarting procedure at coasting condition for a rotational angle sensorless PMSM," *IEEJ J. Ind. Appl.*, vol. 3, no. 2, pp. 131–137, Nov. 2014.
[21] S.-K. Sul and S. Kim, "Sensorless control of IPMSM: past, present, and future," *IEEJ J. Ind. Appl.*, vol. 1, no. 1, pp. 15–23, 2012.
[22] Y.-C. Kwon, S. Kim, and S.-K. Sul, "Six-step operation of PMSM with instantaneous current control," *IEEE Trans. Ind. Appl.*, vol. 50, no. 4, pp. 2614–2625, Jul./Aug. 2014.
[23] T. Yamakawa, S. Wakao, K. Kondo, T. Yoneyama, S. Taniguchi, and S. Mochiduki, "Starting procedure of rotation sensorless PMSM at coasting condition for railway vehicle traction," *IEEJ Trans. Ind. Appl.*, vol. 127, no. 7, pp. 700–706, 2007.

Dong-Woo Seo received the B.S. degree in electronic engineering from Kyung Hee University, Suwon, South Korea, in 2014 and the M.S. degree in electrical and computer engineering from Ajou University, Suwon, South Korea, in 2019.

Since 2019, he has been with the Hyosung, Seoul. His current research interests include power conversion and motor drive systems.

Yeongsu Bak (S'14) received the B.S. and M.S. degrees in electrical and computer engineering from Ajou University, Suwon, South Korea, in 2014 and 2016, respectively. He is currently working toward his Ph.D. degree in Electrical and Computer Engineering at Ajou University, Suwon, South Korea.

His research interests include grid-connected systems and matrix converters.

Kyo-Beum Lee (S'02–M'04–SM'10) received the B.S. and M.S. degrees in electrical and electronic engineering from Ajou University, Suwon, South Korea, in 1997 and 1999, respectively, and the Ph.D. degree in electrical engineering from Korea University, Seoul, South Korea, in 2003.

From 2003 to 2006, he was with the Institute of Energy Technology, Aalborg University, Aalborg, Denmark. From 2006 to 2007, he was with the Division of Electronics and Information Engineering, Chonbuk National University, Jeonju, South Korea. In 2007, he joined the Department of Electrical and Computer Engineering, Ajou University. His research interests include electric machine drives, renewable power generation, and electric vehicle applications.

Dr. Lee is an Associate Editor for the IEEE TRANSACTIONS ON POWER ELECTRONICS, the *Journal of Power Electronics*, and the *Journal of Electrical Engineering and Technology*.